Langmuir

Article

pubs.acs.org/Langmuir

Biomineralization of Hydroxyapatite on DNA Molecules in SBF: Morphological Features and Computer Simulation

Takayuki Takeshita,[†] Yoko Matsuura,[†] Shuichi Arakawa,[†] and Masami Okamoto*,[†]

[†]Advanced Polymeric Nanostructured Materials Engineering, Graduate School of Engineering, Toyota Technological Institute, 2-12-1 Hisakata, Tempaku, Nagoya 468 8511, Japan

ABSTRACT: The hydroxyapatite (HA) formation on the DNA molecules in SBF was examined. After immersion for four weeks in SBF at 36.5 °C, the HA crystallites of ∼1−14 μm in diameter grew on the surface of DNA molecules. Various morphologies were successfully observed through scanning electron microscopy analysis. The Ca/P mol ratio (1.1−1.5) in HA was estimated by energy dispersive X-ray analysis. Original peaks of both of DNA and HA were characterized by Fourier transform infrared spectroscopy. The molecular orbital computer simulation has been used to probe the interaction of DNA with two charge-balancing ions, i.e., $CaOH^+$ and $CaH_2PO_4^+$. The adsorption enthalpy of the two ions on ds-DNA and/or ss-DNA having large negative value (∼ −60 kcal/mol per charge-balancing ion) was the evidence for the interface in mineralization of HA in SBF.

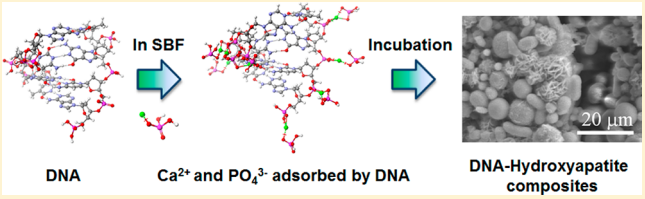

1. INTRODUCTION

When a large bone deficiency occurs by accidents or illnesses, the patient's Quality of Life is adversely affected because of the difficulties in creating new tissue or failing organs for regeneration. One of the most promising approaches toward this direction is to bond to living bone on scaffolds—highly engineered structures that act as a temporary support for bone which facilitate the regeneration of the target tissues without losing the three-dimensional stable structure.[1−3]

Composites based on polymers and ceramics are being developed with the aim to increase the mechanical scaffold stability and to improve tissue interaction. These scaffolds can locally release growth factors or antibiotics and enhance bone ingrowth to treat bone defects and even support wound healing. The composite systems combining advantages of polymers and ceramics seem to be a promising choice for bone tissue engineering.[2,4−7]

Bioactive materials are bonded to living bone by the formation of hydroxyapatite ($Ca_{10}(PO_4)_6(OH)_2$): HA) on its surface when implanted into the living bone. Kokubo et al. proposed that the in vivo osteoconductivity of a material could be predicted from the apatite formation on its surface by using simulated body fluid (SBF) having ion concentrations nearly equal to those of human blood plasma.[8] The osteoconductivity of a variety of scaffolds were investigated, e.g., HA, apatite-wollastonite containing glass-ceramics,[9] polylactide, and their combinations.[5−7]

However, the research on the osteoconductivity of biopolymers is at its infancy. Double-stranded DNA (ds-DNA) is a biological polymer, which consists of nucleotides and phosphate grope. The ds-DNA is one of the most promising biopolymers at the forefront of the emerging clinical and medical applications because of the genetic material and the center of attention in transfection. In addition, the DNA molecules are covered with inorganic minerals; in the process of biomineralization, they might form bioactive nanocomposites that could be regulated. The nanocomposites are expected to be used as gene vehicles because of their good adsorption, high transfection efficiency, and nontoxicity.[10−13] The DNA release from HA mineral coating with different Ca/P ratios on polymeric substrates (such as polystyrene[10] and poly(lactide-*co*-glycolide)[11]) was reported by Shen et al.[10] The composition of HA minerals led to the different mineral stability and, in turn, the release rates of bound DNA. The DNA/HA nanocomposites are expected to pave the way for a new inorganic carrier in gene therapy.

To our knowledge, there are few reports on the morphological development of HA on the DNA templates without polymeric substrates in SBF.[14,15] In this study, the inorganic HA formation on the surface of DNA molecules in SBF was investigated with the aim of directing bone regeneration and the DNA delivery for bone tissue engineering. We also examined the computer simulation to provide insight into the structure and stability of DNA during adsorption of charge-balancing ions in the initial stage of the biomineralization, which is very difficult to obtain from experiment.

2. EXPERIMENTAL SECTION

2.1. Materials. In this study, ds-DNA from salmon tastes (Sigma-Aldrich: D1626) was used. The weight-average molecular weight (M_w) was 1.3 × 10^6 Da possessing 2000 base pairs together with a high aspect ratio (approximate strand length of ∼680 nm[16] and diameter of ∼2 nm[17]). The guanine-cytosine (G-C) content was reported to be 41.2%. As a reference, a natural HA (n-HA) from calf bones was

Received: July 16, 2013
Revised: August 22, 2013
Published: August 27, 2013

purchased from Eccera Ltd., Japan (particle diameter of ~1 μm, Ca/P molar ratio of 1.64).

2.2. Preparation of SBF. Milli-Q ultrapure (18 MΩcm, total organic carbon (TOC) < 20 ppb) water was added into plastic beaker under magnetic stirring. The water in the beaker was heated up to 36.5 °C. All reagents for mineralization were purchased from Nacalai Tesque, Kyoto. The mineralization solution, designated as SBF, (NaCl, 136.8 mM; $NaHCO_3$, 4.2 mM; KCl, 3.0 mM; $K_2HPO_4{\cdot}3H_2O$, 1.0 mM; $MgCl_2{\cdot}6H_2O$, 1.5 mM; $CaCl_2$, 2.5 mM; Na_2SO_4, 0.5 mM; Tris base, 50 mM) was adjusted to the pH 7.40 precisely using 1.0 M of HCl.

2.3. Biomineralization and Characterization. 0.5 g of ds-DNA and 50 mL of SBF were mixed at ambient temperature for 24 h. The solution was incubated at 36.5 °C. After four weeks, a white precipitate (designated as DNA-HA) was yielded in the solution. The precipitate was collected after centrifuge at a speed of 5000 rpm for 5 min and washed by ultrapure water for 3 times. Subsequently, freeze-drying (FDU-2200, Eyela Ltd.) was performed under 20 Pa at −80 °C.

The morphology was observed through field emission scanning electron microscope (FE-SEM: SU6600, Hitachi Ltd.) equipped with elemental analysis by energy dispersive X-ray spectrometry (EDX: INCA x-act, Oxford instruments). The operated accelerating voltage was 10 kV and the specimens were coated with a thin layer of gold and palladium (Au/Pd 6:4) with a thickness of ~20 nm.

Wide angle X-ray diffraction (WAXD) analysis was performed for the precipitated DNA-HA, using an Mxlabo X-ray diffractometer (MAC Science Co; 3 kW, graphite monochromator, CuKα radiation (λ_x = 0.154 nm), operated at 40 kV and 20 mA) at room temperature. Samples were scanned in fixed time mode with counting time of 2 s under diffraction angle 2θ in the range of 1−70°.

Fourier transform infrared (FTIR) spectra were collected from 4000 cm^{-1} to 400 cm^{-1} at 1 cm^{-1} nominal resolution using a FTIR spectrometer (FT-730, Horiba Ltd.) equipped with a MCT detector in transmission mode. The spectra were obtained by averaging 25 scans with a mean collection length of 1 s per spectrum. The background spectra used for reduction were collected with sample. The homogeneous mixture of KBr powder and sample (powder) in the weight ratio 99:1 were prepared.

The thermal behavior was determined by thermogravimetric/differential thermal analysis (TG/DTA 6300, Seiko Instruments Inc.) in the temperature range of 25−900 °C at a heating rate of 5 °C/min under dry air with a flow rate of 260 mL/min. Sample weight of DNA-HA was normalized at 3.0 mg. The ds-DNA before biomineralization (pristine ds-DNA) was used for a control.

The surface charge characteristic of the ds-DNA molecules in water (0.1 wt %) was determined by electrophoresis at 25 °C (Zetasizer Nano ZS, Malvern Instruments, UK) by the technique of laser Doppler anemometry. The method involved adjusting the pH of the suspension in the range of 2−12 by using dilute HCl and NaOH (Nacalai Tesque, Kyoto). All measurements were performed for three replicates and averaged to get the final value. n-HA in water (0.1 wt %) was measured to understand the surface charge characteristic of the precipitated HA from SBF.

2.4. Model Construction for Computer Simulation. Using molecular mechanics force field (MM3) (Scigress, v 2.4.0, Fujitsu Ltd.),[18] in this study, we proposed the molecular structures of ds-DNA possessing four DNA nucleotides (nts) containing individual nucleotide bases (adenine (A), thymine (T), G and C) comprising the following sequences: 5′-ACGT-3′; 5′-ACGT-3′. The duplex is perfectly matched in the modeled ds-DNA. By taking their van der Waals radii into account, the optimization of the molecular structure was based on minimization of the total energy of the molecular system. The charge densities of each atom were estimated by molecular orbital (MO) program using semiempirical parametric method (PM6) charges (Scigress, v 2.4.0).[19] The water molecules were described by the flexible single-point charge (SPC) model[20] for the biomineralization process in SBF. The heat of formation using PM6, in which the dominant interactions are electrostatic, as is the case here, also calculated the adsorption enthalpy.

3. RESULTS AND DISCUSSION

3.1. Surface Charge Characteristics. The phosphate groups of ds-DNA molecules possess a negative charge (PO_2^-). The zeta potential values for the surface of the ds-DNA are negative over the entire pH range from 3 to 11 and even more smaller negative (~ −40 mV) at a lower pH value, which may be attributed by the protons acquired by the phosphate groups on the acid side (Figure 1). Furthermore, the values decrease

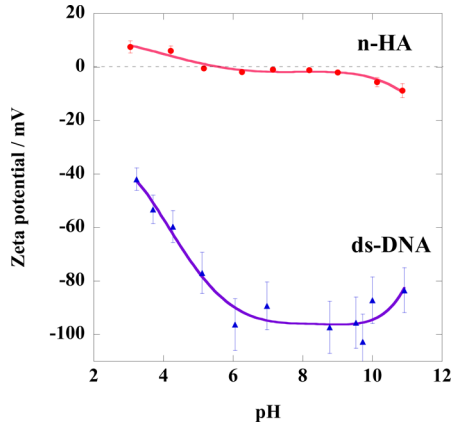

Figure 1. Zeta potential versus pH of ds-DNA and n-HA.

with continuous increase to attain −100 mV at pH 9.72. Beyond pH 10.0, the zeta potential values increase again, presumably due to the two differently charged substituted purine groups.[21]

The main reason for DNA-HA sediment is due to the interaction between negatively charged phosphate (PO_2^-) groups along the backbone of the ds-DNA and Ca^{2+}, which deposited calcium ions, in turn, interacting with phosphate ions (PO_4^{3-}) in the SBF and forming HA. The HA then grew spontaneously accompanied by consuming the calcium and phosphate ions to form apatite.[10,11,13,22] For comparison, the results of the zeta potential measurements of n-HA are shown in Figure 1. The isoelectric point (I_p) of n-HA has the pH range from 5 to 8, where the zeta potential values remain constant ~ −0.2 to −0.8 mV.[23] In the pH range 5−8, both positively and negatively charged species are present on the surface of the n-HA particles.[24] On dispersion into water, the n-HA particles might have various ions on their surfaces (e.g., Ca^{2+}, $CaOH^+$, PO_4^{3-}, HPO_4^{2-}, $H_2PO_4^-$, and $CaH_2PO_4^+$). The positive surface charge is attributed to the increasing adsorption of H^+ or the loss of OH^-,[25] and vice versa in case of the negative surface charge. The highest (+7.6 mV at pH 3.05) and lowest (−8.8 mV at pH 10.86) values are found for n-HA. In both pH regions, the n-HA particles are stabilized electrostatically due to the high surface charge.[26]

3.2. Morphological Features and Structural Analyses. Figure 2a shows the FE-SEM images of the DNA-HA sediment collected after biomeneralization for four weeks in SBF. The DNA-HA mainly exhibits spherical structure with a mean size from 1 to 14 μm. This suggests coprecipitated ds-DNA containing mineral coatings.[10,11]

On the other hand, in the enlarged view (Figure 2b), we clearly observe leaf flake-like morphology near the spherical shaped particles. The thickness of the leaf flake range 0.3−0.5 μm is induced. This morphology is different from the spherical structure. This may imply multistep growth where at first small

dx.doi.org/10.1021/la402589j | Langmuir 2013, 29, 11975−11981

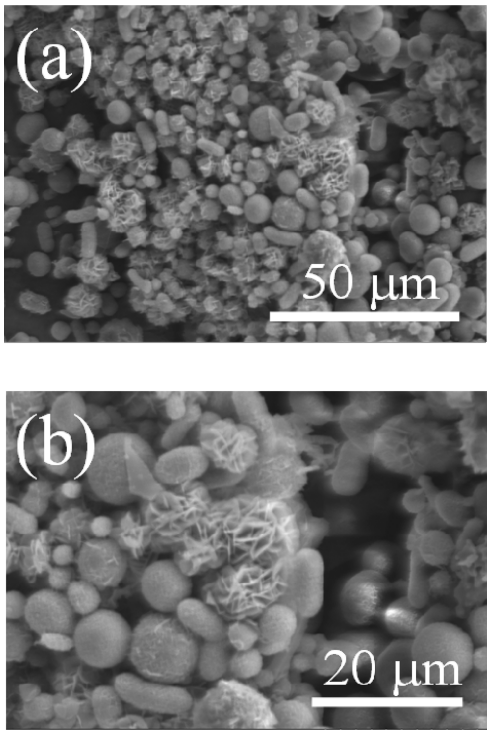

Figure 2. FE-SEM images showing DNA-HA sediment collected after biomeneralization for four weeks in SBF: at (a) low and (b) high magnification.

nuclei occur with the help of the ds-DNA molecules and then overgrow radially from the center with the direction of growth along the crystallographic direction. The chemical composition of the surfaces was analyzed by EDX. The Ca/P molar ratio of the DNA-HA sediment exhibits some range 1.1−1.5, implying that this value is much lower as compared with that of a stoichiometric amount (i.e., 1.67) due to the incorporation of ds-DNA molecules inside the sediment.

After immersion of ds-DNA molecules for 3 days up to week, no apatite formation occurred despite the fact that the SBF is supersaturated condition in aqueous solution. The existence of some incubation time for apatite nucleation is speculated. However, the reproducibility is poor because of the super-saturated solution of the SBF.

The WAXD pattern of the DNA-HA sediment exhibits broad peaks at $2\theta \sim 26°$ (0.34 nm) and ~32° (0.28 nm), which corresponds to (002) and (211) planes, respectively (Figure 3a). A small remnant shoulder around ~33° is assigned to the (300) plane. The standard diffraction pattern of stoichiometric HA (PDF2: 01−072−1243) is also presented as reference (Figure 3b). The peaks derived from ds-DNA could not be observed clearly in the diffraction peaks. Carbonated-substituented HA shows reflections at $2\theta = 26°$ and 32° due to the diffraction occurring from (112) and (300) planes,[11] which overlap well with the pattern of DNA-HA.

Figure 4 shows FTIR spectrum of DNA-HA. Original peaks of both ds-DNA and HA are characterized. The sensitive bands at 1699 cm^{-1} (stretching mode of guanine: ν(C═O)), 1658 and 1648 cm^{-1} (stretching mode: ν(C═C) and ν(C═N)), and 1236 cm^{-1} (asymmetric stretching mode: $\nu_{as}(PO_2^-)$ are attributed to the ds-DNA.[27,28] The sensitive bands at 1093 cm^{-1} ($\nu_3(PO_4^{3-})$), 1031 cm^{-1} ($\nu_3(PO_4^{3-})$), 601 cm^{-1} ($\nu_4(PO_4^{3-})$), and 561 cm^{-1} $\nu_4(PO_4^{3-})$ are attributed to

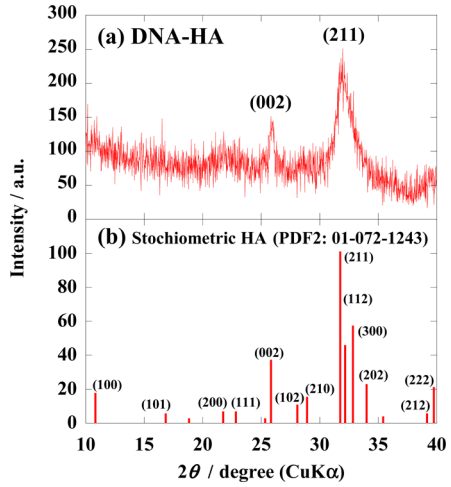

Figure 3. WAXD pattern of (a) DNA-HA sediment and (b) standard diffraction pattern of stoichiometric HA (PDF2: 01−072−1243).

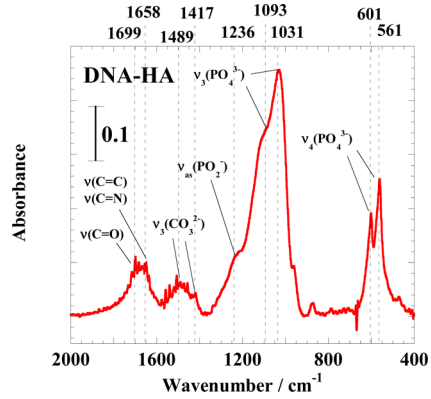

Figure 4. FTIR spectrum of DNA-HA sediment collected after biomeneralization for four weeks in SBF in the region of 400−2000 cm^{-1}.

HA.[29] A band located at 3450 cm^{-1} was assigned to the structural OH stretching mode (ν(OH)) from both ds-DNA and HA (data not shown).

The bands at 1489 cm^{-1} ($\nu_3(CO_3^{2-})$) and 1417 cm^{-1} ($\nu_3(CO_3^{2-})$) appeared.[30,31] That is, the phosphate groups or hydroxyl groups in HA crystallites replaced the carbonate acid in SBF accompanied with the formation of carbonate hydroxyapatite. This result might be consistent with the broad peaks in the WAXD pattern, which indicate low crystallinity by incorporation of carbonate acid into HA via an anion exchange reaction.

3.4. Thermal Properties. The TGA curve, derivative analysis (DTG), and DTA of the DNA-HA sediment and the pristine ds-DNA are shown in Figure 5. The pristine ds-DNA lost absorbed water in the temperature range 50−120 °C, accompanied by the endothermic peak (Figure 5c and d). A significant mass loss (~58%) above 230 °C is observed, accompanied by the three corresponding exothermic peaks at 228, 508, and 653 °C, which are due to the pyrolysis and/or decomposition of ds-DNA[32] (Figure 5c). In contrast, DNA-HA indicates the weight loss of ~13% after the evaporation of water from the DNA-HA sediment (50−200 °C) (Figure 5b). The sd-DNA in the sediment decomposes in two stages, with a weight loss of 10% between 200 and 586 °C and a weight loss of 3% from 586 up to 800 °C, accompanied with the small

dx.doi.org/10.1021/la402589j | Langmuir 2013, 29, 11975−11981

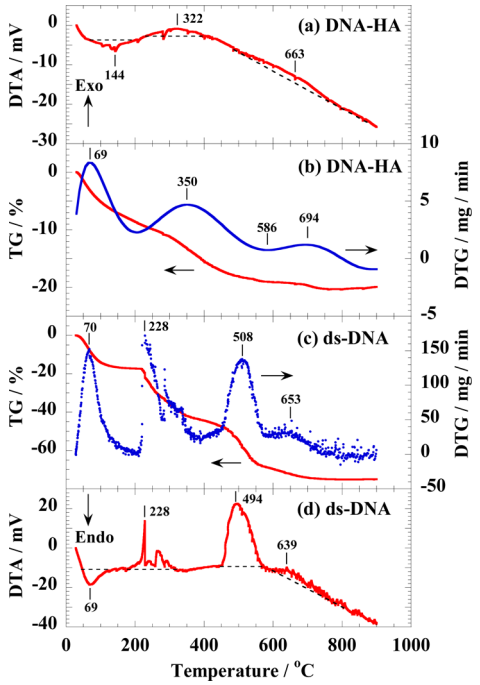

Figure 5. TGA curve, derivative analysis (DTG) and DTA of (a, b) DNA-HA sediment and (c, d) pristine ds-DNA.

exothermic peaks (Figure 5a). At the same time, we find that the two peak temperatures (i.e., 350 and 694 °C) of the ds-DNA degradation in the DNA-HA sediment are shifted higher as compared with that of the pristine ds-DNA (i.e., 228, 494, and 639 °C) (*cf.* DTG curves). The excellent thermal stability of HA beyond the temperature 1000 °C is well-known in the literature.[33] The thermal stability of the incorporated ds-DNA in DNA-HA is much better than that of the pristine ds-DNA, despite the HA formation having nonstoichiometric amount (Ca/P = 1.1−1.5). The calculated weight ratio of ds-DNA/HA in the DNA-HA sediment is *ca.* 18/82 by taking the absorbed water and the combustion residue of the pristine ds-DNA into account.

3.5. Adsorption Enthalpy on Two DNA Strands. To understand the generic adsorption in terms of the electrostatic attraction between the positively charged ions (Ca^{2+}, $CaOH^+$, and $CaH_2PO_4^+$) and negatively charged phosphate (PO_2^-) groups along the backbone of the DNA strand in the initial stage of the biomineralization, here we compare results obtained from the simulation of the systems having $CaOH^+$ and $CaH_2PO_4^+$ as charge-balancing ions. The single-stranded (ss)-DNA is modeled as well ds-DNA, and overall system is built. Figure 6a shows the ss-DNA with four DNA nts (5′-ACGT-3′) before positively charged ion adsorption. Clearly, four $CaH_2PO_4^+$ ions significantly alter the conformation of ss-DNA compared to the corresponding structure in its initial state. The corresponding configuration after adsorption of ions on the ss-DNA backbone was extracted from the final simulation snapshot as shown in Figure 6b-d. The conformation is conserved over the duration of MO simulation, indicating that minimization of the total energy regarding heat of formation has arisen from adoption of this new configuration consisting of the ss-DNA bases, deoxyribose, and the phosphate backbone. The estimated adsorption enthalpy (ΔH_{ad}) values are presented in Table 1. The ΔH_{ad} values are calculated by using the following equation:

$$\Delta H_{ad} = \Delta H_{complex} - (\Delta H_{DNA} + \Delta H_{ion}) \quad (1)$$

where the $\Delta H_{complex}$ value is the heat of formation (in kcal mol^{-1}) of the ss-DNA-ion and/or ds-DNA-ion complexes (such as ss-DNA-$(CaOH)_4$, ss-DNA-$(CaH_2PO_4)_4$, ds-DNA-$(CaOH)_8$, ds-DNA-$(CaH_2PO_4)_8$, and so on) after adsorption, and ΔH_{DNA} and ΔH_{ion} are the isolated components, respectively. The water molecule was also examined as a reference molecule and the overall system was built as well. The calculated results show that the ΔH_{ad} value in ss-DNA-$(CaOH)_4$ and ss-DNA-$(CaH_2PO_4)_4$ are strongly attractive (−239 to −267 kcal/mol)) as compared with that of ss-DNA-$(H_2O)_4$ (−62 kcal/mol). Those complexations are more stable than the isolated DNA molecules.

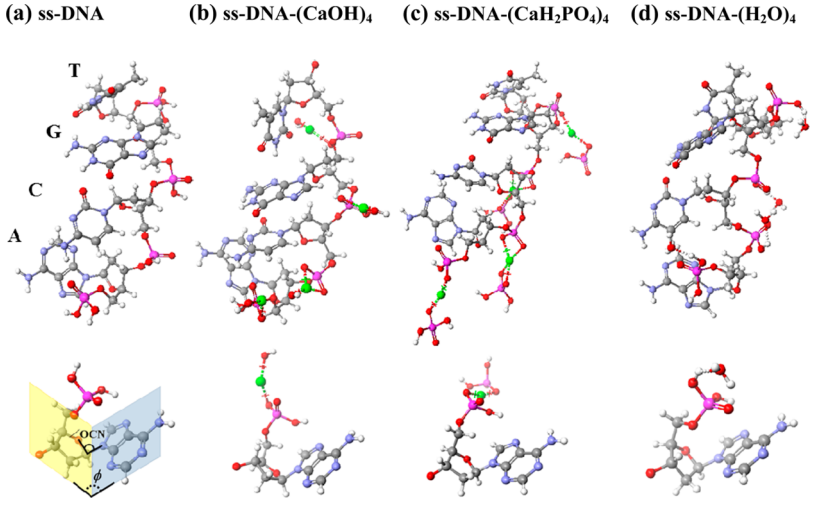

Figure 6. Configuration of ss-DNA with four DNA nts: (a) before charge-balancing ion adsorption (initial state); after adsorption of (b) four ($CaOH^+$)s; (c) four ($CaH_2PO_4^+$)s; (d) four H_2O molecules extracted from the final simulation snapshot. Atom colors: O (red), H (white), C (gray), N (blue), P (pink), and Ca (light green). For visualization of the dihedral angle (ϕ), the deoxyribose and base have been shaded light blue and light yellow, respectively, in the inset of (a). The bond angle ($\angle_{O-C-N}$) between sugar and adenine has been highlighted. Other bases (T, G, and C) have not been displayed.

dx.doi.org/10.1021/la402589j | *Langmuir* 2013, 29, 11975−11981

Table 1. Heat of Formation of Components and Adsorption Enthalpy of DNA-Ion Complexes

molecules	heat of formation/kcal mol^{-1}	ΔH_{ad}/kcal mol^{-1}
ss-DNA	−1200	-
ds-DNA	−2445	-
$CaOH^+$	−57	-
$CaH_2PO_4^+$	−274	-
H_2O	−54	-
ss-DNA-$(CaOH)_4$	−1695	−267 (−67)[b]
ss-DNA-$(CaH_2PO_4)_4$	−2535	−239 (−60)[b]
ss-DNA-$(H_2O)_4$	−1478	−62 (−16)[b]
ds-DNA-$(CaOH)_8$	−3417 (−972)[a]	−516 (−65)[b]
ds-DNA-$(CaH_2PO_4)_8$	−5188 (−2743)[a]	−551 (−69)[b]
ds-DNA-$(H_2O)_8$	−2973 (−528)[a]	−96 (−12)[b]

[a]The values in the parentheses are calculated from ($\Delta H_{complex} - \Delta H_{ds\text{-}DNA}$). [b]The values in the parentheses are calculated per charge-balancing ion.

For visualization of the dihedral angle (ϕ), the deoxyribose and base (adenine) have been shaded light blue and light yellow, respectively, in the inset in Figure 6a. The bond angle ($\angle_{O-C-N}$) between 2-deoxyribose and base has also been displayed. The bond angles of each base against the plane of the 2-deoxyriboses exhibit certain inclination ranging from 105° to 109° for each base in the initial state. There seem to be no significant differences between these angles and those after complexation (Table 2). For better understanding, the dihedral

Table 2. Bond (O−C−N) and Dihedral Angles of Each Base against the Plane of the Deoxyriboses in DNA-Ion Complexes

molecules	bases	bond angles/°	dihedral angles/°
ss-DNA (initial state)	A: adenine	105.1	112
	C: cytosine	106.8	84
	G: guanine	108.0	101
	T: thymine	109.8	101
ss-DNA-$(CaOH)_4$ [-495][a]	A	106.5	107
	C	105.9	93
	G	106.9	114
	T	108.7	119
ss-DNA-$(CaH_2PO_4)_4$ [-1335][a]	A	104.4	120
	C	104.6	59
	G	106.8	87
	T	109.7	98
ss-DNA-$(H_2O)_4$ [-278][a]	A	106.0	92
	C	106.2	71
	G	107.8	108
	T	109.0	96

[a]The values (in kcal mol^{-1}) in the brackets are difference calculated from ($\Delta H_{complex} - \Delta H_{ss\text{-}DNA}$).

angle should be discussed in which the angles are altered to some extent by the differences caused by the stabilized structure after complexation with different charge-balancing ions. For ss-DNA-$(CaH_2PO_4)_4$ as compared with ss-DNA-$(CaOH)_4$, the structure can be discerned from the heat of formation that may be calculated in terms of the difference between $\Delta H_{complex}$ and $\Delta H_{ss\text{-}DNA}$ values, displayed in Table 2. The ion size might affect the conformation of the phosphate backbone and hence the base−base distance and excluded volume correlation.

For ds-DNA-ion complexations, the same features are seen in the corresponding case of ss-DNA-ion complexations after adsorption. The main difference is the configuration of ds-DNA, where the DNA duplex is matched through 5′- or 3′-terminal sequence, which are stabilized by hydrogen bonding between intra-DNA base pair and base-stacking. When the complexation with $CaH_2PO_4^+$, the DNA strands undergo some extent of the collapse between intra-DNA base pairs, accompanied by the conformational change of the phosphate backbone. With greater enthalpy calculated from ($\Delta H_{complex} - \Delta H_{ds\text{-}DNA}$), the large ion size might disrupt the DNA strands with base-stacking because of the more stable complexation (Table 1). These results confirm the importance of the complexation in changing the DNA structure. For this reason, we could observe the repositioning of the individual nucleotide bases before and after complexation by charge-balancing ions (Figure 7). The simulations also demonstrate the somewhat

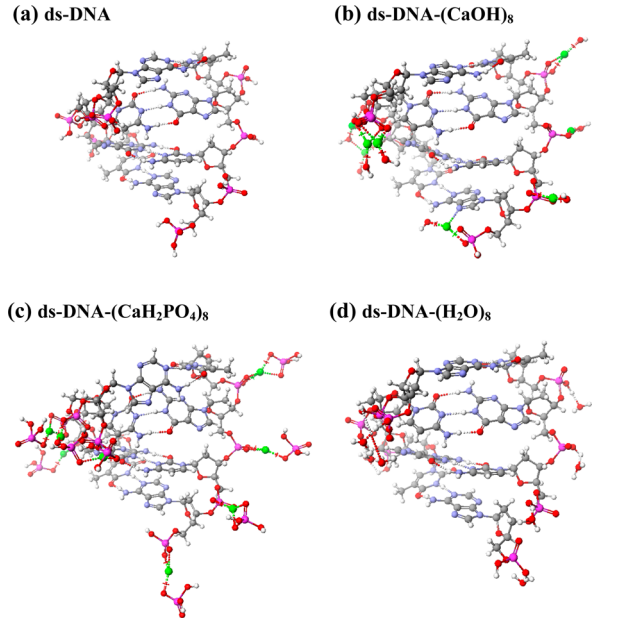

Figure 7. Extracted configuration from the final simulation snapshot of (a) ds-DNA, where the DNA duplex is matched through 5′- or 3′-terminal sequence and after adsorption of the charge-balancing ions: (b) eight ($CaOH^+$)s; (c) eight ($CaH_2PO_4^+$)s; (d) eight H_2O molecules. Color-coding is the same as in Figure 6

changed groove structure of ds-DNA without damaging the structural integrity of the helical strands.[34] The addition of eight charge-balancing ions to ds-DNA leads to a significant increase in ΔH_{ad} as well as $\Delta H_{complex}$ (Table 1). The strong adsorption enthalpy is the main factor in determining the effectiveness of the interface in mineralization of HA, accompanied by the large exotherm per one DNA-strand (∼ −260 kcal/mol). We postulate that the negatively charged PO_2^- groups on the ds-DNA act as nucleating sites and HA crystal growth front as well.

4. CONCLUSIONS

We have demonstrated the HA formation on the ds-DNA molecules in SBF at 36.5 °C. The DNA-HA sediment collected after biomeneralization for four weeks exhibited mainly spherical structure with a mean size from 1 to 14 μm presumably due to the coprecipitated ds-DNA containing

dx.doi.org/10.1021/la402589j | Langmuir 2013, 29, 11975−11981

mineral coatings. The leaf flake-like morphology near the spherical shape particles was observed. The calculated weight ratio of ds-DNA/HA in the DNA-HA sediment was *ca.* 18/82 as revealed by TG/DTA analysis. We have discussed the adsorption enthalpy to clarify the interaction of DNA with ions and the nucleation and growth of HA by MM/MO simulation. Owing to the large negative value (−60 to −69 kcal/mol per charge-balancing ion) in adsorption enthalpy of ions ($CaH_2PO_4^+$ and $CaOH^+$) on ss-DNA and/or ds-DNA, the HA crystal growth spontaneously accompanied by consuming the calcium and phosphate ions to form apatite was suggested.

AUTHOR INFORMATION

Corresponding Author

*Tel: +81-528091861, fax: +81-528091864, E-mail: okamoto@toyota-ti.ac.jp (M. Okamoto).

Author Contributions

The manuscript was written through contributions of all authors. All authors have given approval to the final version of the manuscripts.

Notes

The authors declare no competing financial interest.

ACKNOWLEDGMENTS

This work was supported by the Grant in TTI as a Special Research Project (2012-14) and the Strategic Research Infrastructure Project of the Ministry of Education, Sports, Science and Technology, Japan (2010-14). The authors wish to thank Medical Dr. Ryoji Ishiki of TTI for his stimulating discussions regarding biomineralization in blood plasma.

REFERENCES

(1) Langer, R.; Vacanti, J. P. Tissue engineering. *Science* **1993**, *260*, 920−926.
(2) Ma, P. X. Scaffolds for tissue fabrication. *Mater. Today* **2004**, *7*, 30−40.
(3) Quirk, R. A.; France, R. M.; Shakesheff, K. M.; Howdle, S. M. Supercritical fluid technologies and tissue engineering scaffolds. *Curr. Opin. Solid State Mater. Sci.* **2004**, *8*, 313−821.
(4) Knowles, J. C. A review article: phosphate glasses for biomedical applications. *J. Mater. Chem.* **2003**, *13*, 2395−2401.
(5) Nejati, E.; Mirzadeh, H.; Zandi, M. Synthesis and characterization of nanohydroxyapatite rods/poly(L-lactide acid) composite scaffolds for bone tissue engineering. *Composites, Part A* **2008**, *39*, 1589−1596.
(6) Li, J.; Lu, X. L.; Zheng, Y. F. Effect of surface modified hydroxyapatite on the tensile property improvement of HA/PLA composite. *Appl. Surf. Sci.* **2008**, *255*, 494−497.
(7) Gay, S.; Arostegui, S.; Lemaitre, J. Preparation and characterization of dense nanohydroxyapatite/PLLA composites. *Mater. Sci. Eng., C* **2009**, *29*, 172−177.
(8) Kokubo, T.; Takadama, H. How useful is SBF in predicting in vivo bone bioactivity? *Biomaterials* **2006**, *27*, 2907−2915.
(9) Kokubo, T.; Shigematsu, M.; Nagashima, Y.; Tashiro, M.; Nakamura, T.; Yamamuro, T. Apatite- and wollastonite-containing glassceramic for prosthetic application. *Bull. Inst. Chem. Res. Kyoto Univ.* **1982**, *60*, 260−268.
(10) Shen, H.; Tan, J.; Saltzman, W. M. Surface-mediated gene transfer from nanocomposites of controlled texture. *Nat. Mater.* **2004**, *3*, 569−574.
(11) Choi, S.; Murphy, W. L. Sustained plasmid DNA release from dissolving mineral coatings. *Acta Biomater.* **2010**, *6*, 3426−3435.
(12) Cheng, B.; Cai, W.; Yu, J. DNA-mediated morphosynthesis of calcium carbonate particles. *J. Colloid Interface Sci.* **2010**, *352*, 43−49.
(13) Sun, B.; Yi, M.; Yacoob, C. C.; Nguyen, H. T.; Shen, H. Effect of surface chemistry on gene transfer efficiency mediated by surface-induced DNA-doped nanocomposites. *Acta Biomater.* **2012**, *8*, 1109−1116.
(14) Ngourn, S.; Butts, H.; Baratham, V.; Gerdon, A. E. Hydroxyapatite biomineralization through structural DNA templates. *Proceedings of the 242nd National Meeting of ACS* **2011**, *242*, 155−INOR.
(15) Ngourn, S; Landry, S; Anderson, J; Gerdon, A. E. Identification of DNA structural motifs for hydroxyapatite binding and biomineralization. *Proceedings of the 240th National Meeting of ACS* **2010**, *240*, 176.
(16) Rosa, M.; Dias, R.; Miguel, M. G.; Lindman, B. DNA-Cationic Surfactant Interactions Are Different for Double- and Single-Stranded DNA. *Biomacromolecules* **2005**, *6*, 2164−2171.
(17) Patil, A. J.; Li, M.; Dujardin, E.; Mann, S. Novel Bioinorganic Nanostructures Based on Mesolamellar Intercalation or Single-Molecule Wrapping of DNA Using Organoclay Building Blocks. *Nano Lett.* **2007**, *7*, 2660−2665.
(18) Mizuno, C.; John, B.; Okamoto, M. Percolated network structure formation and rheological properties in nylon 6/clay nanocomposites. *Macromol. Mater. Eng.* **2013**, *298*, 400−411.
(19) Stewart, J. J. P. Optimization of parameters for semiempirical methods V: Modification of NDDO approximations and application to 70 elements. *J. Mol. Model.* **2007**, *13*, 1173−1213.
(20) Berendsen, H. J. C.; Grigera, J. R.; Straatsma, T. P. The missing term in effective pair potentials. *J. Phys. Chem.* **1987**, *91*, 6269−6271.
(21) Schellman, J. A.; Stigter, D. Electrical double layer, zeta potential, and electrophoretic charge of double-stranded DNA. *Biopolymers* **1977**, *16*, 1415−1434.
(22) Zhang, Q.; Mochalin, V. N.; Neitzel, I.; Hazeli, K.; Niu, J.; Kontsos, A.; Zhou, J. G.; Lelkes, P. I.; Gogotsi, Y. Mechanical properties and biomineralization of multifunctional nanodiamond-PLLA composites for bone tissue engineering. *Biomaterials* **2012**, *33*, 5067−5075.
(23) Parks, G. A. *Advanced chemistry series*; McGraw Hill: New York, 1967; Vol *67*, p 121.
(24) Sokolova, V.; Epple, M. Inorganic nanoparticles as carriers of nucleic acids into cells. *Angew. Chem., Int. Ed.* **2008**, *47*, 1382−1395.
(25) Skartsila, K.; Spanos, N. Surface characterization of hydroxyapatite: Potentimetric titrations coupled with solubility measurements. *J. Colloid Interface Sci.* **2007**, *308*, 405−412.
(26) *Zeta Potential of Colloids in Water and Waste Water*; ASTM Standard D 1985, pp 4187−4182.
(27) Malins, D. C.; Gilman, N. K.; Green, V. M.; Wheeler, T. M.; Barker, E. A.; Anderson, K. M. A cancer DNA phenotype in healthy prostates, conserved in tumors and adjacent normal cells, implies a relationship to carcinogenesis. *Proc. Natl. Acad. Sci. U.S.A.* **2005**, *102*, 19093−19096.
(28) Brewer, S. H.; Annthireya, S. J.; Lappi, S. E.; Drapcho, D. L.; Franzen, S. Detection of DNA Hybridization on Gold Surfaces by Polarization Modulation Infrared Reflection Absorption Spectroscopy. *Langmuir* **2002**, *18*, 4460−4464.
(29) Murphy, W. L.; Kohn, D. H.; Mooney, D. J. Growth of continuous bonelike mineral within porous poly(lactide-co-glycolide) scaffolds in vitro. *J. Biomed. Mater. Res.* **2000**, *50*, 50−58.
(30) Chang, M. C.; Tanaka, J. FT-IR study for hydroxyapatite/collagen nanocomposite cross-linked by glutaraldehyde. *Biomaterials* **2002**, *23*, 4811−4818.
(31) Xu, G. F.; Aksay, I. A.; Groves, J. T. Continuous crystalline carbonate apatite thin films. A Biomimetic approach. *J. Am. Chem. Soc.* **2001**, *123*, 2196−2203.
(32) Wang, L.; Yoshida, J.; Ogata, N.; Sasaki, S.; Kajiyama, T. Self-Assembled Supramolecular Films Derived from Marine Dexyribonucleic Acid(DNA)-Cationic Surfactant Complexes: Large-Scale Preparation and Optical and Thermal Properties. *Chem. Mater.* **2001**, *13*, 1273−1281.
(33) Liu, D. M.; Troczynski, T.; Tseng, W. J. Water-based sol-gel synthesis of hydroxyapatite: process development. *Biomaterials* **2001**, *22*, 1721−1730.

(34) Rothemund, P. W. Folding DNA to create nanoscale shapes and patterns. *Nature* **2006**, *440*, 297−302.